ABSTRACT

The research presented within this paper focuses on two 9-meter CX-100 wind turbine blades, designed by Sandia National Laboratories (SNL) and manufactured by TPI Composites Inc.. The key difference between the blades was that the one blade contained no known defects, while the other blade had wave defects of controlled geometry inserted at specified locations along the blade length. The defect-free blade and defect blade were tested at the National Renewable Energy Laboratory (NREL) National Wind Technology Center (NWTC) using a schedule of cycles at increasing load level until failure was detected. Digital image correlation (DIC) was used as a structural health monitoring (SHM) technique, along with several other methods including: shearography, acoustic emission, fiber optic strain sensors, foil strain gages, thermal imaging, and PZT sensors for comparison. The paper compares the sensing results of the different SHM approaches to detect the defects and subsequent damage from the initial fatigue cycle to final failure.

INTRODUCTION

The increasing demand for wind power has led to a significant increase in the number and size of wind-turbine blades manufactured globally. As the number and physical size of turbines deployed grows, the probability of manufacturing defects being present in composite turbine blades also increases. As capital blade costs and operational and maintenance expenses increase in ever larger turbine systems, the need for inspection of the structural health of large-scale turbine blades during operation and testing increases. The focus of the research was a defect referred to as a “wave defect”, “wrinkle”, or “out-of-plane buckle”. The wave defect has been

Christopher Niezrecki, Peter Avitabile, Julie Chen, James Sherwood, and Troy Lundstrom, University of Massachusetts Lowell, Lowell, MA; Scott Hughes and Michael Desmond, National Renewable Energy Laboratory, Boulder, CO; Alan Beattie, Mark Rumsey and Bruce LeBlanc, Sandia National Laboratory, Albuquerque, NM; Sandra M. Klute, Luna, Blacksburg, VA; Rudy Werlink, National Aeronautic and Space Administration, Kennedy Space Center, FL; John Newman Laser Technology Inc., Norristown, PA

recognized by many in the wind industry as a defect that is difficult to prevent in the manufacturing process, difficult to detect (versus a poor bond or dry section), and highly likely to cause unexpected failure. As a result, design knockdowns are overly conservative to account for such defects and even minor defects that are discovered after manufacturing can result in a blade needing repair or being discarded. Both approaches drive up the costs of blades and lead to a significant decrease in the economic competitiveness of wind turbines. In support of the U.S. Department of Energy's effort to develop affordable, reliable domestic wind power, this research investigated the interrogation of manufacturing-induced defects in wind turbine blades by using a variety of sensing technologies.

DESCRIPTION OF THE EXPERIMENT

The research presented within this paper is focused on a fatigue test of a 9-meter, CX-100 wind turbine blade fabricated at TPI Composites Inc.. What is unique about this blade is that it possesses six known embedded defects in the spar cap laminates having an amplitude of 3 mm located at 3.5m, 5m, and 6m from the root of the blade and aspect ratios of 5, 10, and 15, respectively. Defects were placed on both the high pressure (HP) and low pressure (LP) sides. More details about the blade construction, the defect geometry, and the composition of the defects can be found in [1, 2]. The blade was tested at NREL's NWTC using a schedule of cycles at increasing load level until failure was detected (see Figure 1a). DIC was used as a SHM technique, along with several other methods, including acoustic emission, fiber optic strain sensors, shearography, foil strain gages, and PZT sensors for comparison.

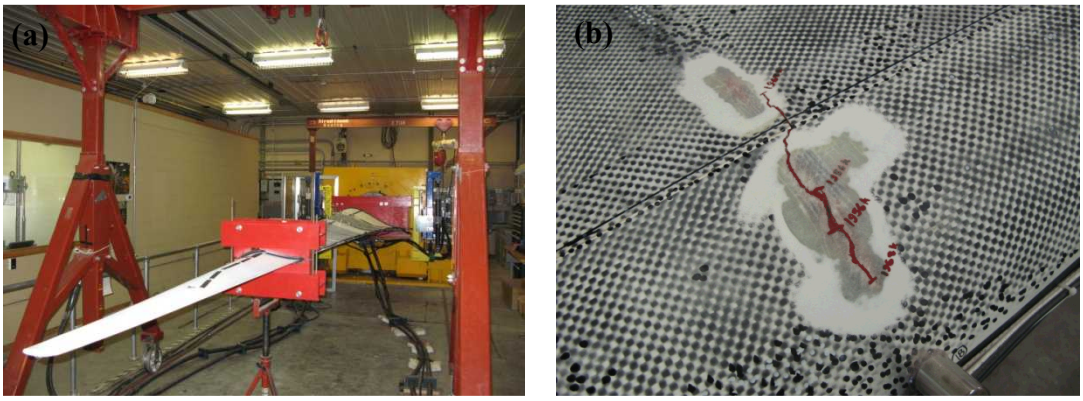

Figure 1 (a) NREL-NWTC flapwise fatigue test setup for 9-meter CX-100 defect blade; (b) structural failure near wave defect at 5m location, after approximately 1.9 million cycles at increasing load levels (the surrounding pattern applied is used for DIC).

An accelerated 1-million cycle design life fatigue load was applied to the blade before increasing loads in discrete steps up to 130% of the target fatigue loads, at which point a 2.5-cm long crack was observed at the 5-m station on the HP surface spar cap, biased towards the leading edge (LE) as shown in Figure 1b. The test ran for approximately 1.9-million cycles before the failure. Full details of the loading levels and duration applied can be found in [2]. A suite of sensor measurements were either made continually or intermittently throughout the fatigue test until and after failure. The different sensor results are now discussed.

BACKGROUND OF DIC AND SETUP

Three-dimensional Digital Image Correlation (3D DIC) is an evolving measurement technique that has only very recently been proposed for wind turbine blade inspection and structural health monitoring [3-9]. 3D DIC is a full field, non contact optical, measuring technique that uses two digital cameras to measure surface geometry, displacement, and strain. All the DIC analysis in this work was performed using GOM's software ARAMIS. To perform these measurements, a stochastic pattern is applied to the surface of interest and a series of photographs (stages) are taken by both cameras as the surface deforms. Strain is computed by comparing the stochastic pattern of the deformed surface to the initial reference measurement of the pattern. Three-dimensional information is extracted using the principles of stereophotogrammetry. DIC can be used for structural health monitoring by comparing current surface geometry, displacement, and strain measurements to baseline measurements made days, months, or even years prior. Monitoring these parameters over time allows for inspection and monitoring of wind turbine structural members. To the authors' knowledge this work represents the first published work to comprehensively compare DIC to other traditional and new sensor technologies on a full-scale wind turbine blade.

Prior to collecting data, the surface of the blade was sanded to remove the glossy gel-coat and a random speckle pattern was applied using paint and markers. For the high-pressure surface (HPS) test, the cameras were mounted to a gantry straddling the blade to provide the required field of view. The test setup with blade, saddle, and applied load (via suspended dead weights) is shown in Figure 2.

Figure 2 (a) Camera bar mounted to overhead gantry; (b) CX-100 blade under load.

RESULTS OF DIC TESTING

For each measurement location, the blade was loaded upwards with a force of 325 lbs. to offset the weight of the saddle (located at 6.75 m). Therefore the only load that the blade experienced was due to its own weight. Five reference images were taken and subsequently the blade was loaded downward by applying a 518 lb. weight to the saddle. An additional five images were captured. Images were taken at one of the six defect locations in the reference (upward loaded) and loaded (downward) positions and then the cameras were repositioned. The test was repeated for each of the six defect locations at a specific number of fatigue cycles.

Six sets of images were taken at a fatigue cycle count of a) 0 cycles; b) 25,603 cycles; c) 755,049 cycles; d) 1,803,350 cycles. The strain computation settings used for Aramis can be found in [1].

Figure 3 shows an example of a representative DIC measurement at the 5.0-m location along the low pressure (LP) side of the CX-100 (virgin blade). The strain across the surface of the blade as indicated by the double-arrow line in Figure 3a is plotted in Figure 3b where the nominal strain away from the defect is compared to the magnitude of the amplified strain at the location of the defect. The results reveal that the defect locations are readily discernible. Each of the locations near the defect has larger than nominal strain.

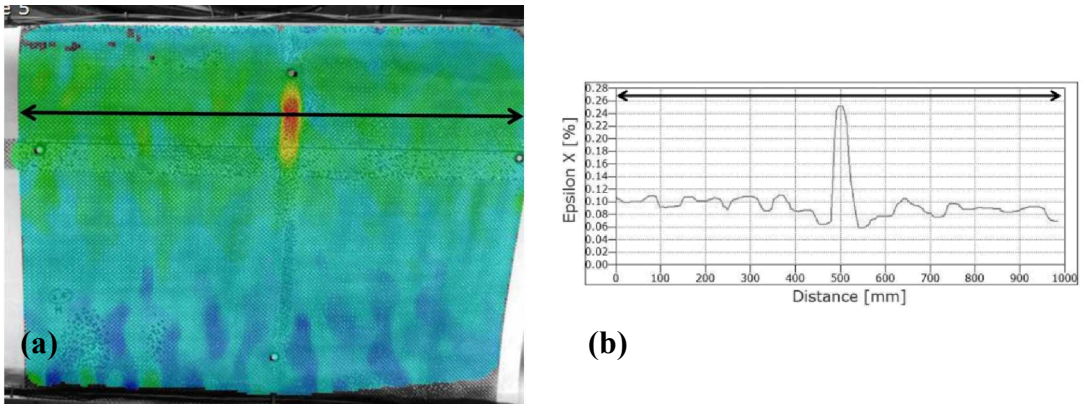

Figure 3 (a) DIC measurement of strain at the 5.0-m location along the LP side of the blade; (b) corresponding strain in a section line passing through the defect location

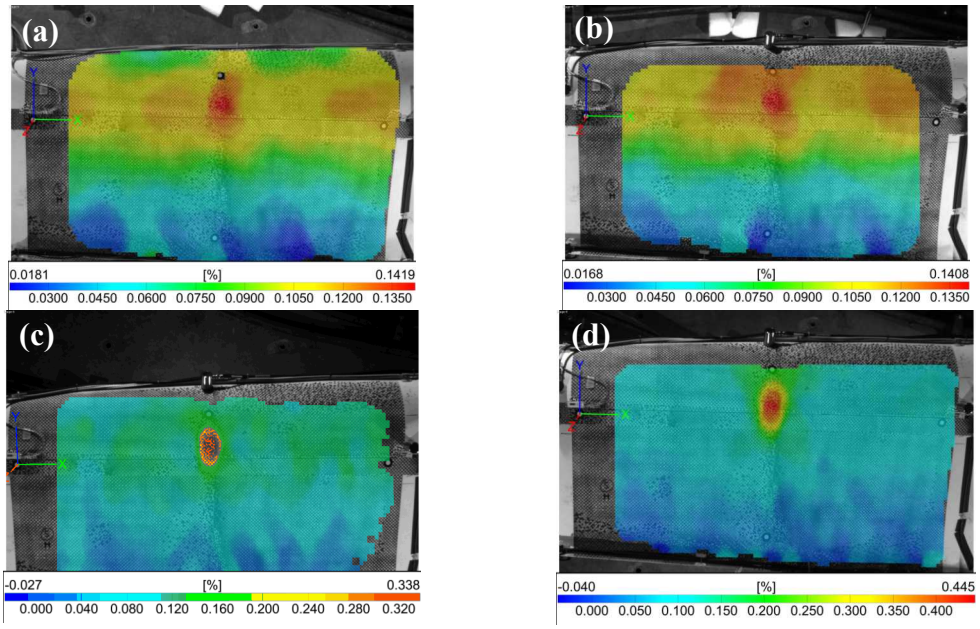

Figure 4 DIC strain contour plots for the 5.0-meter HP section at (a) 0 cycles; (b) 25,603 cycles; (c) 755,049 cycles; (d) 1,803,350 cycles

As the blade was cycled, the strain amplification in the vicinity of the defect became more apparent as is shown in Figure 4 for the 5m HP side, defect location

(area where failure first occurred). The images for the other regions are similar and have been omitted for brevity. The results of the work confirm DIC is an effective method of measuring full-field displacement, strain, and locating cracks and wave defects on wind turbine blades.

BACKGROUND OF SHEAROGRAPHY AND SETUP

Shearography non-destructive testing uses a common path imaging interferometer show the first derivative of the out-of-plane deformations on a structure with a resolution as small as 20 nm in response to an applied load or thermal excitation. While the laser light does not penetrate below the surface of the test part, the selected stressing method (such as heat) does penetrate and allows the detection and measurement of deep as well as surface anomalies such as fiber waves, impact damage, delaminations, cracks and breaking adhesive bonds. Shearography cameras have a built-in laser light source to illuminate an area on the test part. The field of view can range from several square inches to several square meters, depending on the maximum allowable defect size. The laser light reflects from the surface of the test part and enters the shearography camera aperture (see Figure 5). A beam splitter and two mirrors are used to create two separate images of the test area, which are combined on a CCD detector. The position of one image with respect to the other image can be adjusted in any direction or amount. The "sheared" laser illuminated image pairs interfere with each other and are referred to as an interferogram. The amount and direction of the image shear offset is referred to as the shear vector and determines the sensitivity of the shear camera to changes in shape on the surface of the test part [10, 11].

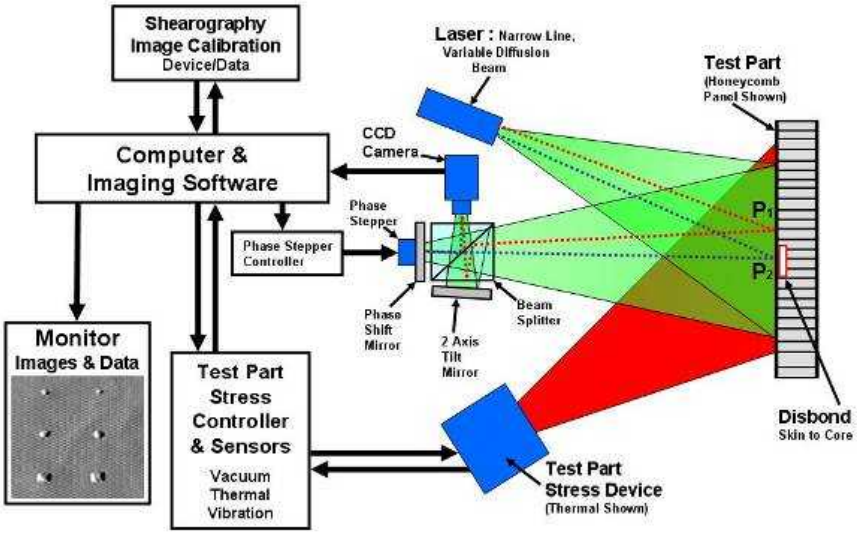

Figure 5 Schematic diagram of a digital shearography NDT system includes the laser and optical elements for test part illumination, beams splitter with a 2 axis tilting mirror, a second mirror with a PZT Phase stepper, CCD camera, and appropriate computer

RESULTS OF SHEAROGRAPHY TESTING

To conduct the shearography testing on the 9 m wind turbine blade, the shearography camera and thermal lamps were attached to an overhead gantry crane

that allowed the team to scan the entire high pressure (HP) side of the blade from the tip to the root. Sequential thermal shearography images were made at every location. The thermal shearography consisted of blade heating for 3 to 14 seconds. The longer heat cycle was used to compensate for the increased distance to target near the blade root. The blade is fixtured pointing up at an angle while the shearography camera scanned at a constant distance above the laboratory floor causing a five foot variation in the distance to target. In addition, the blade shell thickness increases closer to the root end. No problems were encountered compensating for the changing distances and fields of view, using the remote control zoom lens and laser diffuser.

Shearography testing was performed twice during the fatigue cycling at 120,000 cycles and 820,000 cycles. The thermal shearography testing was accomplished using a shear vector of 0.5 inch (12.7mm) orthogonal to the trailing edge. The thermal stress was applied after capturing the reference image. The final image was taken when the real-time phase map fringe order reached zero. All embedded wave defects were detected using shearography prior to the start of the fatigue tests. Shearography tests of all the embedded wave defects taken at 120,000 cycles revealed extensive crack formation on the HP side fiber waves, with no such crack formation detected on the LP side. The crack at 5m on the HP side, as seen in Figure 6, shows extensive crack formation considerably beyond the axial (chord-wise) length of the defect. The blade ultimately failed at this 5 m location. The results demonstrate that thermal shearography has excellent capability to detect out-of plane fiber wave defects and the capability to detect low cycle fatigue damage.

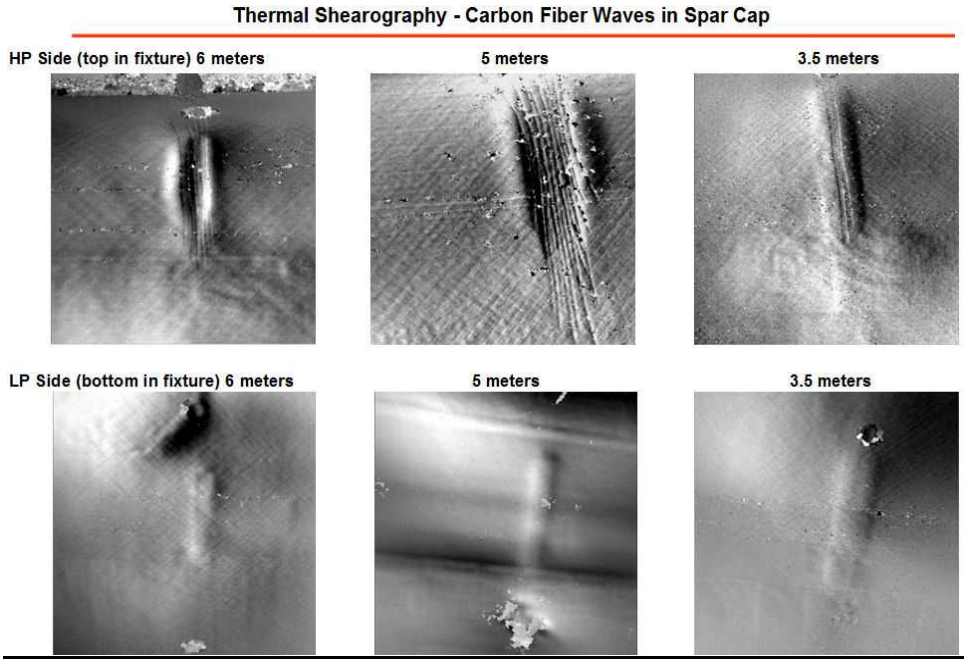

Figure 6 Thermal shearography inspection of all HP and LP fiber wave defects after 120,000 fatigue cycles. Cracks are seen at all three defects on the HP side.

BACKGROUND OF FIBER OPTIC STRAIN SENSORS AND SETUP

Over the past several decades, optical fiber sensing techniques have been developed which make possible the measurement of strain profiles from sensors embedded within a composite material. Optical fiber is ideal for this application – it is lightweight, small in diameter, immune to EMI, and composed of fused silica, which is materially compatible with most composites used in the industry. Froggatt et. al. showed that the Rayleigh scatter signal reflected from the fiber can be used to form a fully distributed fiber sensor using a technique known as Optical Frequency Domain Reflectometry (OFDR) [12]. Recent work using OFDR has shown strain measurements with spatial resolution as fine as a few millimeters [13, 14, 15] enabling a detailed and sensitive measure of the strain profile within a composite material.

In the work described here, based on Klute et. al. [16] and Pedrazanni et. al. [17], off-the-shelf optical fiber was embedded into four of the composite layers comprising the carbon fiber spar cap of the CX-100 blade. The first of four fibers was integrated in the +/-45 layer directly under the defects, with the second, third, and fourth fibers integrated into the triax layers immediately above the defects. An additional fiber was also bonded to the surface of the completed blade. Strain measurements were made with Luna's commercially available OFDR instrument every 2.5mm along the length of the blade (from 2m-7m and back) during the manufacture and subsequent testing of the blade.

RESULTS OF FIBER OPTIC STRAIN SENSOR TESTING

The embedded optical fibers were monitored during the manufacturing process of the blade. The defects were evidenced by regions of concentrated strain immediately upon pulling vacuum during the Vacuum Assisted Resin Transfer and Molding (VARTM) process. The completed blade was interrogated to determine residual strain, shown in Figure 7. Localized regions of tension on the order of 1000με are apparent at each of the defect locations in the blades as the fiber runs out from 2.5m to 7m and back.

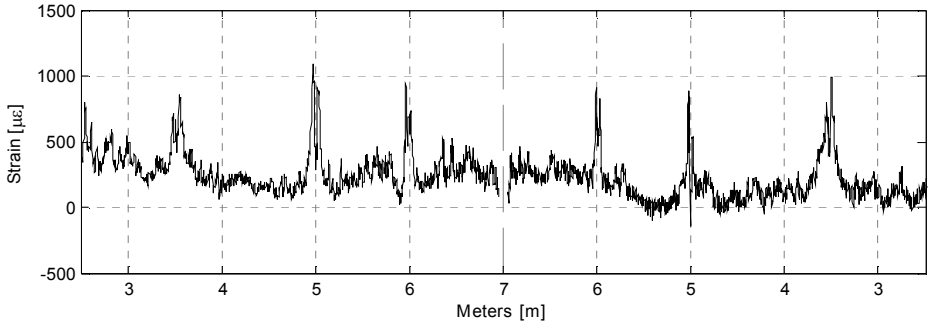

Figure 7. Residual strain in fiber embedded under the defects in the HP side of the blade.

Prior to fatigue cycling, the blade was mounted in a test stand for static testing under a ~500 lb load. Figure 8 shows corresponding distributed fiber optic strain data compared with co-located electrical foil gages for the HP and LP spar cap from 0.5m to 7m locations. Readily apparent in the fiber optic strain data are regions of

high localized strain at blade locations that correspond to the known internal defects introduced in the blade during manufacture. Local strain in these regions is approximately three times in amplitude that of the surrounding strain field. The widths of the peaks correlate well with the widths of the defects. Regions of large strain gradients on either side of the defect indicate the extreme stress concentration caused by the simulated 3mm out-of-plan waviness and the ability of the distributed optical measurement technique to resolve critical small scale features that might go undetected with single point sensors.

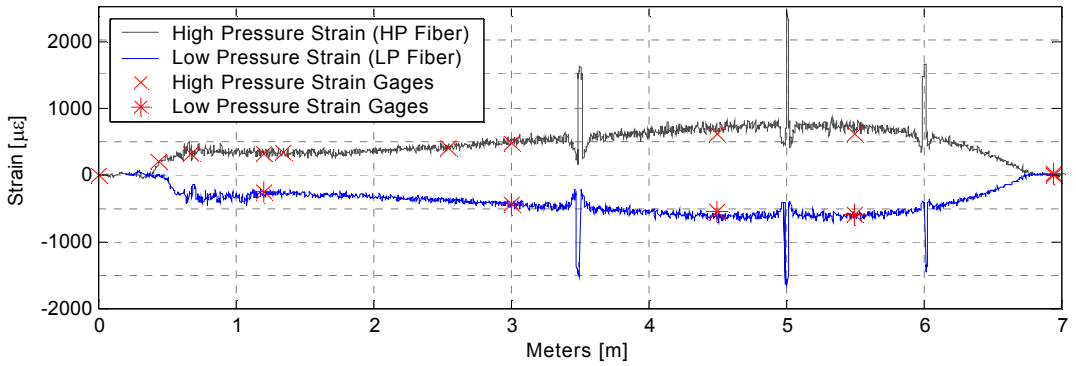

Figure 8. Surface Mounted Fiber Optic Strain Data with Co-Located Foil Strain Gages on CX-100 under 500lb Load Prior to Fatigue Test along Spar

Distributed strain was measured, under various load conditions, at intervals during the fatigue testing. The blade failed at 1.968 million cycles due to a defect on the high-pressure side of the blade. Luna's no-load measurements identified significant growth in the critical defect by cycle 614,000, which correlates with the time that low-level acoustic emission was first detected from the blade. Damage was not visible on the surface of the blade until 1.95 million cycles (see Figure 9).

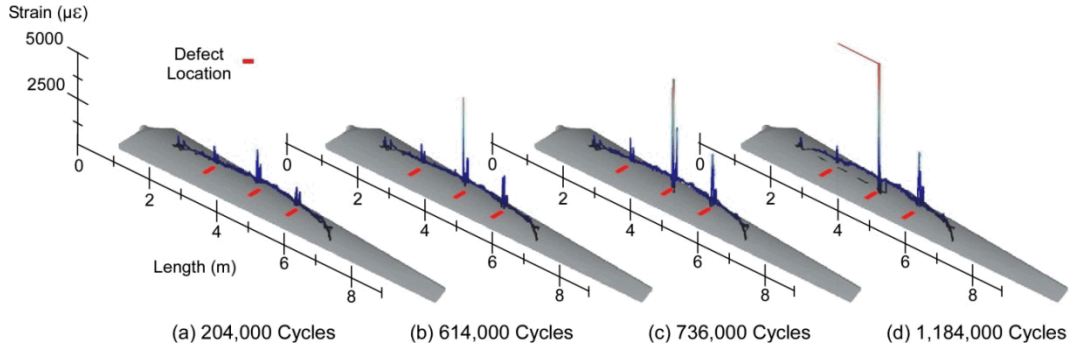

Figure 9. Distributed strain measured at four different cycle counts during fatigue testing. The data presented are for strain in the sensing fiber embedded under the defects within the carbon fiber spar cap. The growth of the defect located at 5 meters on the high pressure side of the blade broke the sensing fiber sometime between (c) 736,000 cycles and (d) 1,184,000 cycles. The blade ultimately failed at this location at 1,968,000 cycles.

BACKGROUND OF PZT SENSORS AND SETUP

The NASA PZT Health Monitoring System results have been previously reported for 9 meter blade (CX-100, TX-100 and BSDS designs) fatigue tests

conducted at the NREL blade testing facility. A collaborative effort between Sandia National Laboratories (SNL) and NASA KSC has been performed to evaluate the viability of a NASA structural health monitoring (SHM) system for wind turbine blades [18]. The system includes a combination of signal data processing and a unique sensor/actuator consisting of piezoelectric (PZT) materials in a thin and highly sensitive configuration. As part of the current test, the objective was to demonstrate the ability of the PZT based NASA KSC health monitoring technology to detect stiffness changes of the 9m wind turbine blade (with manufacturing wave defects) as it is fatigue cycled to failure. Five PZT sensors and one PZT actuator on the blade were attached to the bottom low pressure (LP) side only–surface facing down as installed in the fixture. The sensor plan view is shown in Figure 10.

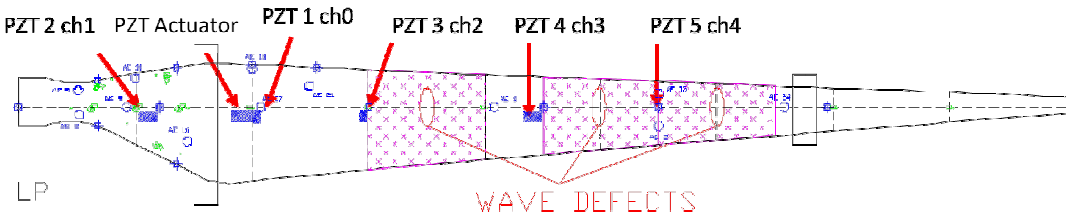

Figure 10. Location of PZT health monitoring sensors and actuator

RESULTS OF PZT SENSOR TESTING

Sensor data was recorded with the PZT actuator energized only while the blade was stopped at planned periodic intervals during the fatigue cycling. Data quantity was affected due to Test cell power outages and Laptop Operating system/data software setup problems which led to a considerable amount of missed data. Full length (20 second) data files were only recorded for the baseline (pre-test) and after failure (post-test). Short (1.5 second) data files were recorded at 1795, 1803 and 1979 kilo-cycles. The measurement history is summarized in Table xx.

Table xx. NASA PZT Health Monitoring System Test Matrix

Data files	Date data taken	Number of fatigue cycles (thousands)	Blade condition
20 seconds channels 0-3	12/14/2011	0	No damage
1.5 seconds ch 0-4	2/17/2012	1795	No visible structural cracks
1.5 seconds ch 0-4	2/21/2012	1803	No visible structural cracks
1.5 seconds ch 0-4	2/29/2012	1979	5m HP crack 165 mm long
20 seconds channels 0-4	3/1/2012	1979	5m HP crack 165 mm long

The frequency response functions (FRFs) between the PZT sensors and actuator are shown in Figure 11 revealing differences in modal peaks before (blue traces) and after (red traces) occurrence of the fatigue crack at the 5 meter location. Unfortunately, the cracking occurred on the opposite side of the blade from the

sensors. The crack was closest to sensor 4 (ch3). The nearly identical traces of the same color were taken at different time windows.

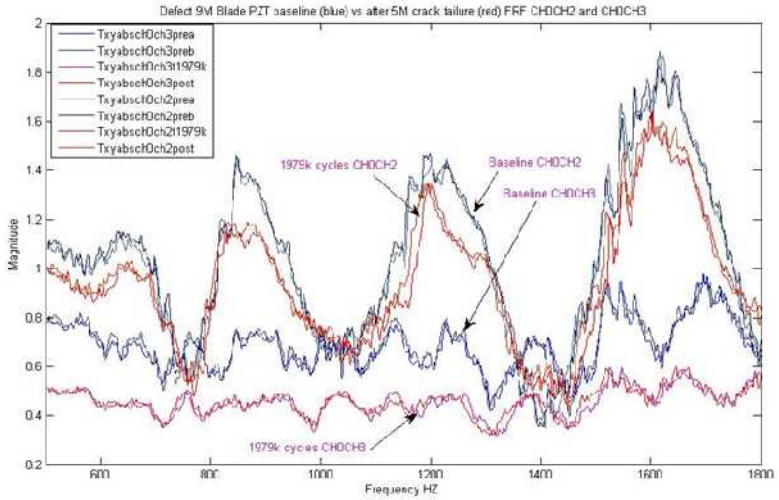

Figure 11. FRF of the PZT sensor/actuators demonstrating a change in the signature past 1979 k-cycles compared to the baseline

Shown in Figure 12 are the FRFs of ch 2 to ch 4 which span the 5m 164 mm long crack showing slight differences in modal peak frequency just before the detection of the surface crack. It should be mentioned that the crack was on the opposite side of the blade (HP side) from the PZT actuator and sensors (LP side) which greatly decreased detect ability. It is recommended that subsequent monitoring should attach a set of actuators and sensors on both sides of a blade to provide an adequate signal. Still, very small changes to the stiffness were detected as indicated by slightly lower frequencies, as seen in Figure 12. Prior blade fatigue test results have shown very detectable frequency shifts due to flaws with an adequate signal (actuator and sensors on the same side of the blade as the defects).

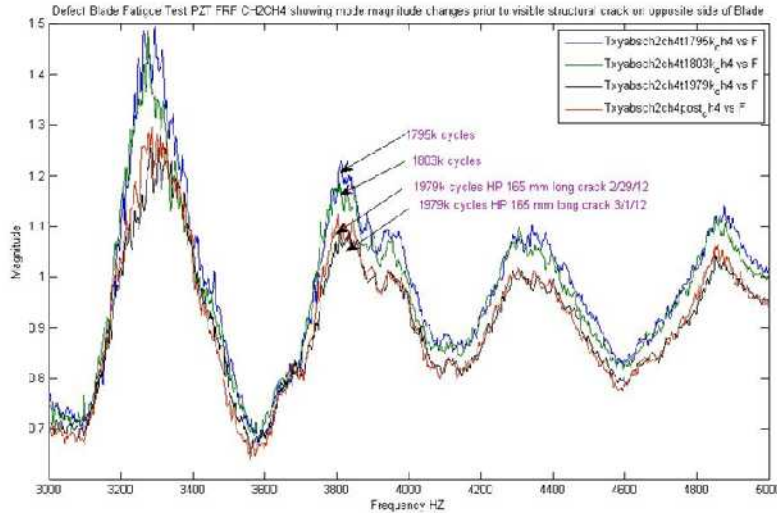

Figure 12. FRF of the PZT sensor/actuators (channel 2 and 4) demonstrating a change in the signature near failure.

BACKGROUND OF THERMAL IMAGING AND SETUP

Discrete thermal imaging of the blade was performed using a FLIR SC640 thermal spectrum camera in the areas of interest. The 40-mm objective lens has spatial resolution accuracy of ±2.0°C. This type of non-destructive evaluation method is useful in determining thermal hot spots or areas where thermal activity is generated. With regards to wind turbine blades, this thermal activity is created primarily from friction of fiber rubbing, matrix cracking, or cracks propagating, which typically occur in areas of high stress and defects.

RESULTS OF THERMAL IMAGE TESTING

The results of the thermal imaging performed are shown in Figure 13 for the wave defect under fatigue loading. It can be seen that the defects emit a clearly detectable amount of thermal energy, on the order of 6°C warmer than the surrounding regions. Although the defect locations were known in this case, it should be clear how thermal imaging can be a useful tool for detecting and locating thermal hot spots and defects. While the exact nature of the defect may not be obvious, having known locations for performing additional non-destructive inspections is very valuable.

Figure 13 – Thermal Image of Out-of-Plane Wave Defect under Fatigue Loading

BACKGROUND OF ACOUSTIC EMISSION AND SETUP

Monitoring the acoustic emission generated by growing flaws allows the detection, location and growth characteristics of the flaws. Such monitoring of wind turbine blades has been conducted at NREL for the last twenty years [19-25]. For this test, a twenty four channel SAMOS AE System running AEwin software (Physical Acoustics Corporation, PAC) was used to monitor the blade during the fatigue test. Twenty three PAC R6I AE sensors were mounted on the blade using a RTV Silicone adhesive. The R6I AE sensor has an integral preamplifier with 40 dB of gain, peak sensitivity near 60 KHz and a useable acoustic bandwidth of approximately 20 KHz to 120 KHz. The AE sensors were attached to the low-pressure (LP) and high-pressure (HP) outer surfaces of the blade. The SAMOS

system was set to detect all AE signals which exceeded an input threshold of 45 dB (178 microvolts out of the sensor).

The AE sensor layout, shown in Figure 14, was designed to surround all the built-in blade embedded defects with at least a triangle of sensors. The sensor positions and the acoustic velocity between the AE sensors were measured before the start of the fatigue test. The average velocity of the acoustic wave along the spar cap of the blade was measured to be 4.0 mm/microsecond. An AE event was defined as the arrival of an acoustic wave at three or more sensors within a time window of 800 microseconds. Both the AEwin software and Sandia-derived programs were involved in the AE source location calculations which used the arrival times from three to six sensors. The energy of an AE event was defined as the sum of the absolute energies of the first three detected AE signals used in the location calculation. These energies are those of the detected signals and are only roughly related to the actual energy of the AE event itself.

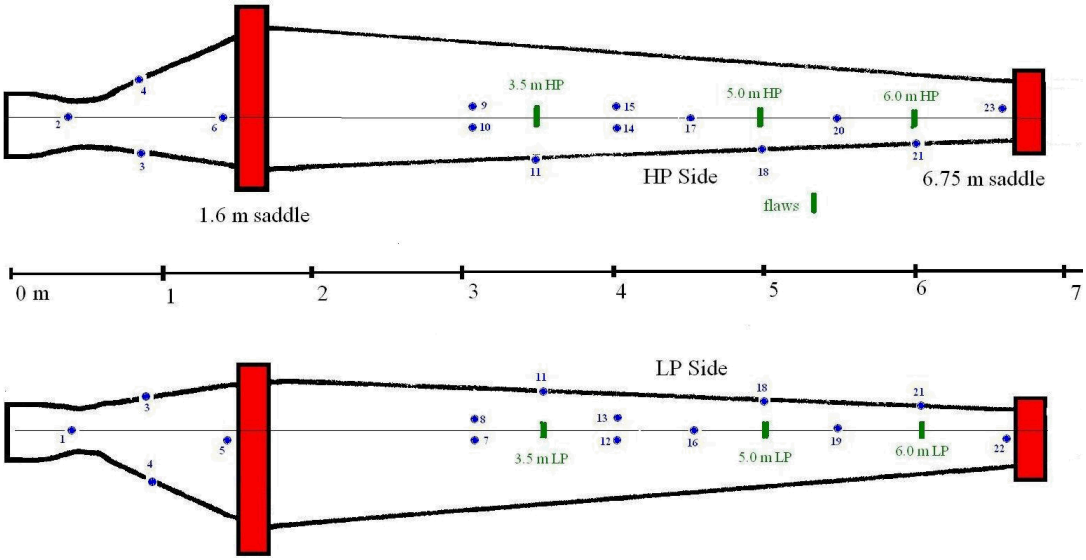

Figure 14 – AE sensor layout for the HP (top) and LP sides (bottom)

Flaw growth in a fatigue test occurs primarily near the maximum stress levels so AE data was recorded only during the time when the loaded blade was in the top and bottom 10% of the peak deflection. AE location calculations were conducted in real-time to allow a continuous record of the AE activity in the blade. Post-test calculations allowed the measurement of relative AE activity in various regions on the blade. It should be noted that the NASA PZT-based SHM instrumentation produced acoustic signals that were detectable in the PAC AE system. The AE system was paused whenever the NASA SHM instrumentation was activated, to prevent recording of these extraneous signals.

RESULTS OF ACOUSTIC EMISSION TESTING

The blade failed after an accumulation of 1,968,186 fatigue cycles. Blade failure occurred near the 5.0-meter flaw when a resultant 5-inch long crack started near the leading edge on the high-pressure tension side of the loaded blade. Most of the AE energy released during the last 20,000 cycles of the test came from the region around the 5 meter defect on the high pressure surface. A map of the AE events and

the AE energy released in the mapped area are shown in Figure 15. The point labeled **fracture** is the AE event which occurred closest in time to the crack initiation. The light-yellow box indicates the approximate location of the blade 5 m defect.

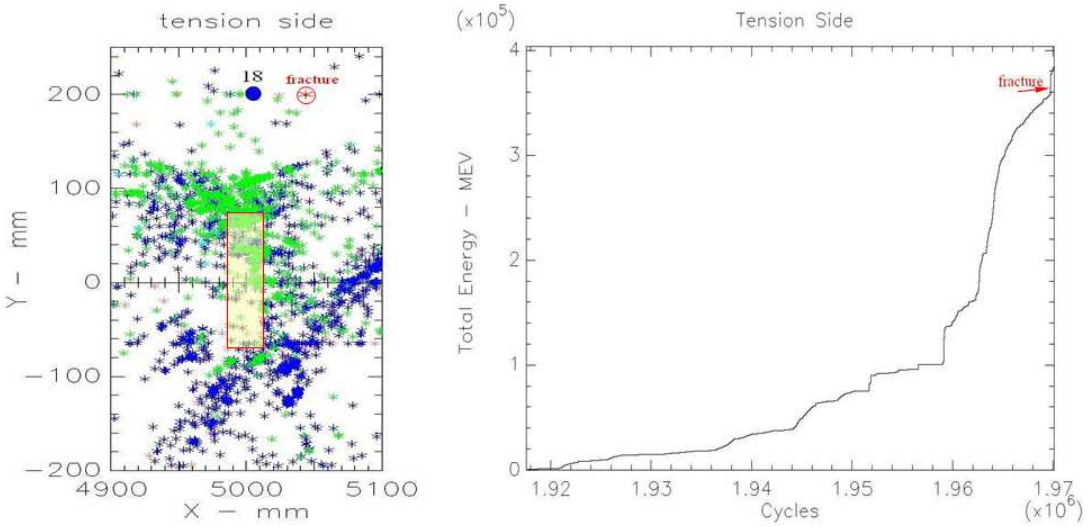

Figure 15 – AE events near the 5 m defect (left) and the corresponding AE energy

For comparison, all the AE events that occurred near the defects at 3.5-meters and 6.0-meters are shown in Figure 16, during this last load block. The light-yellow boxes shown in the left two figures outline the approximate areas of the defects. The figure on the right shows the AE energy released in the rectangular bold-outlined area near the 6-meter defect.

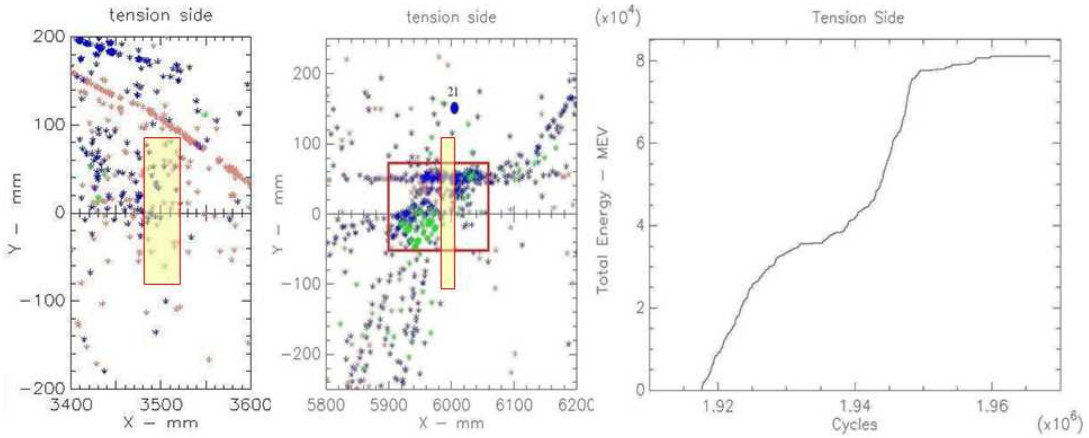

Figure 16 – AE events near the 3.5 m and 6m defects (left) and the corresponding AE energy emitted near the 6 m location.

BACKGROUND OF METAL FOIL STRAIN SENSORS AND SETUP

A total of 27 foil strain gages were installed on the blade. These were single-axis gages of the type WK-05-250BG-350 with a 350-ohm resistance nominal. They were oriented in the spanwise direction, 0-deg, and connected in a three-wire quarter-bridge configuration. The gages were used to collect local strains at 11 different spanwise locations. A single point static load was applied at the outboard 6.75-m saddle location in order to calibrate the sensitivity of the gages with respect

to bending moment, which was used to determine the applied moments during fatigue testing.

RESULTS OF METAL FOIL STRAIN TESTING

A representative timeline of the flapwise fatigue test is provided in Figure 17 for a single strain gage. Prior to the primary failure at the 5-m defect location, no significant structural changes were observed.

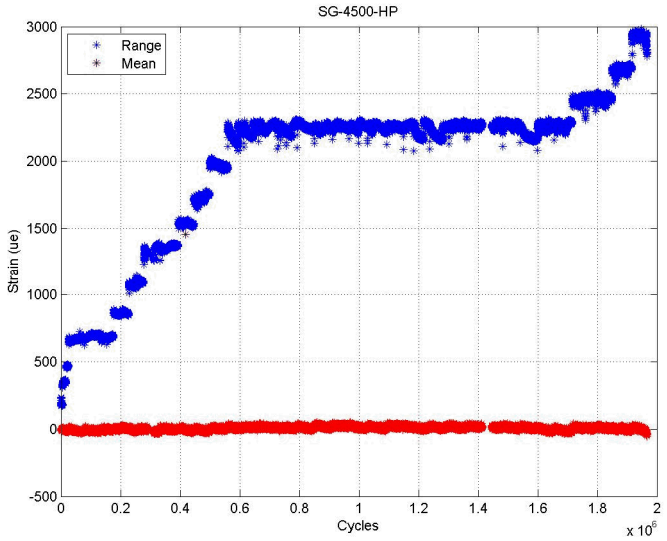

Figure 17 – Representative Strain of Single Foil Gage during Fatigue Testing

A comparison study was performed by Luna Inc. between the fiber optic strains and traditional foil strain gages with good correlation, as shown in Figure 8. The fiber optics reported that there were stress risers on the order of 2-3 times higher in the defect areas (illustrated by the spikes at 3.5, 5 and 6-m) as compared to surrounding areas. Unfortunately, due to placement constraints, no foil gages were installed at the defect locations for verification. The closest gages were located half a meter away and did not exhibit this behavior, demonstrating the improved distributed sensing.

CONCLUSION

The fatigue test performed on a 9m wind turbine blade with embedded defects has provided a unique test bed from which several different sensing approaches have been evaluated and compared including: DIC, shearography, acoustic emission, fiber optic strain sensors, foil strain gages, thermal imaging, and PZT sensors. DIC, shearography, and thermal imaging are non-contacting techniques that provided a clear full-field identification and assessment of the location of the embedded defects and subsequent cracking. Fiber optic strain sensing was able to interrogate the length of the entire embedded fiber, clearly revealing strain amplification at the locations of the embedded defects. An acoustic emission sensor suite was able to monitor the blade throughout the fatigue test and was able

to identify energy emissions from cracks associated with the defects. Likewise, the distributed PZT sensors were able to measure subtle changes to the stiffness of the turbine blade as the structure was damaged. Both the PZT sensors and the foil gage strain sensors were able to infer a change in the structure, but are not able to localize or as easily quantify the damage as effectively as the other sensing approaches. This project has advanced not only our understanding of the variety of sensing approaches but when implemented as a quality assurance tool, can help to minimize wave defect formation, reduce their detrimental impact, and detect them earlier. The research also has contributed to practical methods and tools that can be used by industry to improve the design, manufacturing process, and nondestructive inspection/structural health monitoring of composite wind turbine blades.

ACKNOWLEDGEMENTS

The authors gratefully appreciate the financial support for this work provided by the Department of Energy (DE-EE001374). Any opinions, findings, and conclusions or recommendations expressed in this material are those of the authors and do not necessarily reflect the views of the DOE.

REFERENCES

1. Leblanc, B., M.S. Thesis, "Non-Destructive Testing of Wind Turbine Blades with Three Dimensional Digital Image Correlation" Univ. of Massachusetts Lowell, Sept. 2011.
2. FINAL TECHNICAL REPORT: "Effect of Manufacturing-Induced Defects on Reliability of Composite Wind Turbine Blades," U.S. Department of Energy Award No. DE-EE0001374; UMass Lowell Report # S51900000011598, August, 2012.
3. LeBlanc, B., Niezrecki, C., Hughes, S., Avitabile, P., Chen, J., and Sherwood, J., "Full Field Inspection of a Wind Turbine Blade Using 3D Digital Image Correlation," Proceedings of the SPIE Symposium on Smart Structures & Materials/NDE for Health Monitoring, San Diego, California, March, 2011.
4. Helfrick, M. and Niezrecki, C., "An Investigation of the use of 3-D Optical Measurements to Perform Structural Health Monitoring," 6th International Workshop on Structural Health Monitoring, Stanford, CA, Sept. 11-13, 2007.
5. Helfrick, M., Niezrecki, C., and Avitabile, P., "Curvature Methods of Damage Detection using Digital Image Correlation," Proceedings of the SPIE Symposium on Smart Structures & Materials/NDE for Health Monitoring, San Diego, California, March, 8-12, 2009.
6. LeBlanc, B., Niezrecki, C., and Avitabile, P., "Structural Health Monitoring of Helicopter Hard Landing using 3D Digital Image Correlation (DIC)," Proceedings of the SPIE Symposium on Smart Structures & Materials/NDE for Health Monitoring, San Diego, California, March, 7-11, 2010.
7. LeBlanc, B., Niezrecki, C., Avitabile, P., Sherwood, J., and Chen, J., "Surface Stitching of a Wind Turbine Blade Using Digital Image Correlation," Proceedings of IMAC-XXX, Jacksonville, FL, January 30 - February 2, 2012.
8. Carr, J., Baqersad, J., Niezrecki, C., Avitabile, P., and Slattery, M., "Dynamic Stress-strain on Turbine Blade using Digital Image Correlation Techniques Part 1 - Static Load and Calibration," Proceedings of IMAC-XXX, Jacksonville, FL, January 30 - February 2, 2012.
9. Carr, J., Baqersad, J., Niezrecki, C., Avitabile, P., and Slattery, M., "Dynamic Stress-Strain on Turbine Blade Using Digital Image Correlation Techniques Part 2 - Dynamic Measurements," Proceedings of IMAC-XXX, Jacksonville, FL, January 30 - February 2, 2012.
10. American Society for Testing and Materials (ASTM) , Standard Practice for Shearography of Polymer Matrix Composites, Sandwich Core Materials and Filament-Wound Pressure Vessels in

Aerospace Applications, E2581-07.
11. Newman, J. and Lindberg, J. “Shearography Inspection of Wind Turbine Blades”, Materials Evaluation ASNT, pp. 829-837, July, 2010.
12. M. Froggatt and J. Moore, “High resolution strain measurement in optical fiber with Rayleigh scatter,” Appl. Opt., 37, 1735-1740 (1998).
13. M. Froggatt, B. Soller, D. Gifford, and M. Wolfe, “Correlation and keying of Rayleigh scatter for loss and temperature sensing in parallel optical networks,” OFC Technical Digest, paper PDP 17 (Los Angeles, March 2004).
14. B.J. Soller, D. K. Gifford, M. S. Wolfe, M. E. Froggatt, M. H. Yu, and P. F. Wysocki, “Measurement of localized heating in fiber optic components with millimeter spatial resolution,” OFC Technical Digest, paper OFN 3, 2006.
15. S. Kreger, D. K. Gifford, M. E. Froggatt, B. J. Soller, and M. S. Wolfe, "High resolution distributed strain or temperature measurements in single- and multi-mode fiber using swept-wavelength interferometry," OFS 18 Technical Digest, Paper ThE42, 2006.
16. Klute, S. M., Sang, A. K., Gifford, D. K., Froggatt, M. E., “Defect Detection During Manufacture of Composite Wind Turbine Blade with Embedded Fiber Optic Distributed Strain Sensor,” SAMPE Fall Technical Conference, Ft. Worth, Texas, Oct. 17-20, 2011.
17. Pedrazzani, J. P., Klute, S. M., Gifford, D. K., Sang, A. K., Froggatt, M. F., “Embedded and Surface Mounted Fiber Optic Sensors Detect Manufacturing Defects and Accumulated Damage as a Wind Turbine Blade is Cycled to Failure”, SAMPE Spring Technical Conference, Baltimore, MD, May 21-24, 2012.
18. PZT Active Frequency Based Wind Blade Fatigue to Failure Testing Results for Various Blade Designs R. J. Werlink [NASA Kennedy Space Center, USA] IWSHM, 8th International Workshop on Structural Health Monitoring 2011 8th IWSHM Paper 2680.
19. Rumsey, M., “NDT, CM and SHM of Wind Turbine Blades at the National Labs,” NREL Wind Turbine Condition Monitoring Workshop, Louisville, CO, Oct. 2009.
20. Rumsey, M., “Sensor Projects at Sandia National Laboratories,” IEA Expert Meeting #56 Smart Structures, Albuquerque, NM, May 2008.
21. Rumsey, M., “Sensor Projects at Sandia National Laboratories,” SNL Wind Turbine Blade Workshop, Albuquerque, NM, May 2008.
22. Paquette, J.; Hughes, S.; van Dam, J.; Johnson, J., “Fatigue Testing of 9 m Carbon Fiber Wind Turbine Research Blades,” AIAA-2008-1350, 46th AIAA Aerospace Sciences Meeting and Exhibit, Reno, NV, January 2008.
23. Paquette, Joshua; van Dam, Jeroen; Hughes, Scott, “Structural Testing of 9 m Carbon Fiber Wind Turbine Research Blades,” AIAA-2007-816, 45th AIAA Aerospace Sciences Meeting and Exhibit, Reno, NV, January 2007.
24. Sutherland, H.; Beattie, A.; Hansche, B.; Musial, W.; Alread, J.; Johnson, J. and Summers, M., "The Application Of Non-Destructive Techniques to the Testing of a Wind Turbine Blade," SAND93-1380, Sandia National Laboratories, Albuquerque, NM, June 1994.
25. Sutherland, H.J.; Musial, W., "The Application of Non-Destructive Techniques to the Testing of a Wind Turbine Blade," WindPower 93 Proceedings, AWEA, Washington, D.C., 1993.